

# In Situ Observation and Electrochemical Study of Encapsulated Sulfur Nanoparticles by MoS<sub>2</sub> Flakes

Wei Tang,<sup>†,‡,§,¶</sup> Zhongxin Chen,<sup>†,§</sup> Bingbing Tian,<sup>†</sup> Hyun-Wook Lee,<sup>\*,||</sup> Xiaoxu Zhao,<sup>†,§</sup> Xiaofeng Fan,<sup>#,¶</sup> Yanchen Fan,<sup>∇</sup> Kai Leng,<sup>†,§</sup> Chengxin Peng,<sup>†</sup> Min-Ho Kim,<sup>||</sup> Meng Li,<sup>○</sup> Ming Lin,<sup>‡</sup> Jie Su,<sup>†,§</sup> Jianyi Chen,<sup>†,¶</sup> Hu Young Jeong,<sup>⊥</sup> Xuesong Yin,<sup>‡</sup> Qianfan Zhang,<sup>∇</sup> Wu Zhou,<sup>◆</sup> Kian Ping Loh,<sup>\*,†,§,¶</sup> and Guangyuan Wesley Zheng<sup>\*,‡</sup>

<sup>†</sup>Department of Chemistry, National University of Singapore, 3 Science Drive 3, 117543 Singapore

<sup>‡</sup>Institute of Materials Research and Engineering, A\*STAR, 2 Fusionopolis Way, Innovis, 138634 Singapore

<sup>§</sup>Centre for Advanced 2D Materials and Graphene Research Centre, National University of Singapore, 6 Science Drive 2, 117546 Singapore

<sup>||</sup>School of Energy and Chemical Engineering and <sup>⊥</sup>UNIST Central Research Facilities and School of Materials Science and Engineering, Ulsan National Institute of Science and Technology (UNIST), Ulsan 44919, Republic of Korea

<sup>#</sup>College of Materials Science and Engineering, Key Laboratory of Automobile Materials of MOE, Jilin University, Changchun 130012, China

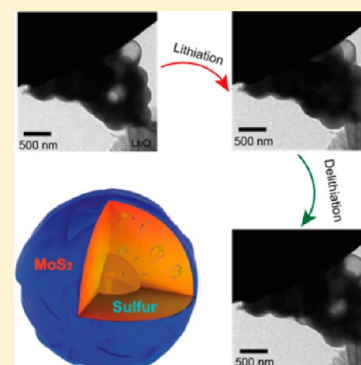
<sup>∇</sup>School of Materials Science and Engineering, Beihang University, Beijing 100191, PR China

<sup>○</sup>School of Power Engineering, Chongqing University, Chongqing, 400044, China

<sup>◆</sup>Materials Science and Technology Division, Oak Ridge National Laboratory, Oak Ridge, Tennessee 37831, United State

## Supporting Information

**ABSTRACT:** Sulfur is an attractive cathode material for next-generation lithium batteries due to its high theoretical capacity and low cost. However, dissolution of its lithiated product (lithium polysulfides) into the electrolyte limits the practical application of lithium sulfur batteries. Here we demonstrate that sulfur particles can be hermetically encapsulated by leveraging on the unique properties of two-dimensional materials such as molybdenum disulfide (MoS<sub>2</sub>). The high flexibility and strong van der Waals force in MoS<sub>2</sub> nanoflakes allows effective encapsulation of the sulfur particles and prevent its sublimation during *in situ* TEM studies. We observe that the lithium diffusivities in the encapsulated sulfur particles are in the order of 10<sup>-17</sup> m<sup>2</sup> s<sup>-1</sup>. Composite electrodes made from the MoS<sub>2</sub>-encapsulated sulfur spheres show outstanding electrochemical performance, with an initial capacity of 1660 mAh g<sup>-1</sup> and long cycle life of more than 1000 cycles.



## INTRODUCTION

The adoption of intermittent renewable energy sources like solar and wind energy, along with the electrification of transportation, demand the development of rechargeable batteries with high energy density and low cost.<sup>1–9</sup> As one of the most promising new battery materials, sulfur can potentially enable lithium batteries to achieve about 5 times the specific energy of today's lithium ion batteries. However, there are still several challenges that need to be addressed before the technology can become practical. Some of the major problems in lithium sulfur batteries include the dissolution of intermediate lithium polysulfides (Li<sub>2</sub>S<sub>x</sub>,  $x > 3$ ) into the electrolytes, the large volume change of sulfur particles after lithiation (~80%), and the insulating nature of sulfur and Li<sub>2</sub>S.<sup>10–16</sup> To date, many efforts have been made to address these issues through trapping of dissolvable lithium polysulfides in conductive matrixes such as mesoporous/microporous/

hollow carbon,<sup>17–22</sup> carbon nanotubes/fibers,<sup>23–26</sup> and conducting polymers.<sup>27–29</sup> Functional groups have also been introduced as the anchor sites to adsorb lithium polysulfides. In particular, polymers,<sup>30–33</sup> functionalized graphene,<sup>34–40</sup> and nitrogen-doped carbon matrixes have been used to enable strong interaction between lithium polysulfides and the polar surface on the electrodes. Similar strategies were also explored using metal oxides,<sup>41,42</sup> sulfides,<sup>43,44</sup> and metal organic frameworks and their derivatives.<sup>45–50</sup>

Despite the many attempts in electrode engineering, so far there has been little *in situ* observation and understanding of the sulfur electrode reaction at the nanoscale, and the few works that have been done are with electrode structures that are difficult to be used in practical batteries.<sup>51,52</sup> Recent

Received: May 30, 2017

Published: July 3, 2017

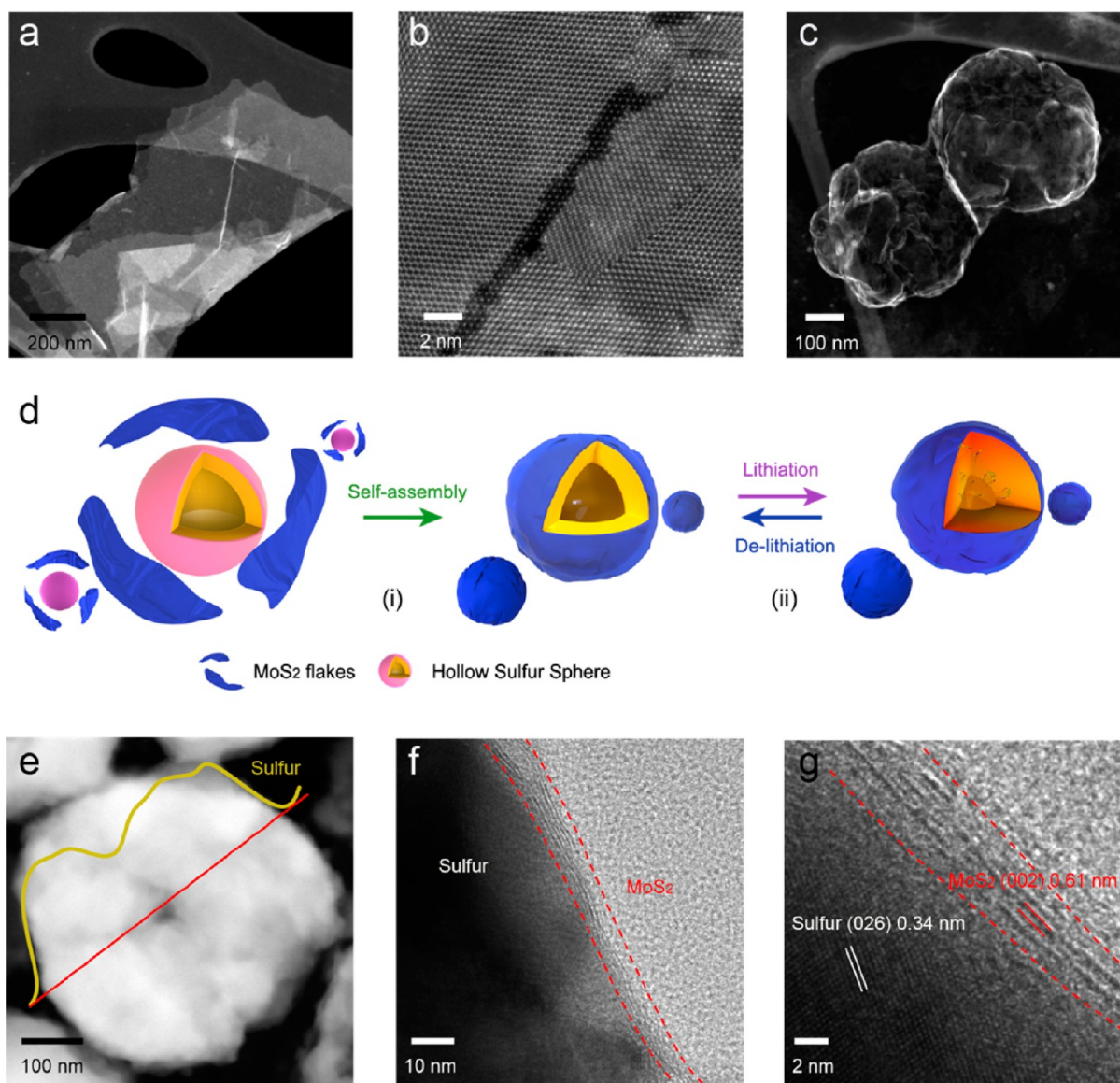


**Figure 1.** Hermetic encapsulation of sulfur spheres by flexible MoS<sub>2</sub> flakes. (a) STEM image of typical MoS<sub>2</sub> flakes and (b) atomic STEM images to show the crystalline structure of MoS<sub>2</sub> flakes. (c) STEM images of hollow MoS<sub>2</sub> cages upon removal of sulfur particles. (d) Schematic of (i) the synthesis process of MoS<sub>2</sub>-encapsulated hollow sulfur sphere, (ii) effective soluble lithium polysulfides entrapment and structural integrity of MoS<sub>2</sub>-encapsulated hollow sulfur sphere upon lithiation/delithiation. (e) STEM image and (f, g) high-resolution TEM images of MoS<sub>2</sub>-encapsulated hollow sulfur sphere. Inset of (e) indicates the line scan EDX signal of sulfur.

progress in two-dimensional (2D) materials provides new opportunities in structure designs that allow us to gain insight into new materials.<sup>53,54</sup> Here we show that the hermetic encapsulation of sulfur particles using MoS<sub>2</sub> nanoflakes generates highly robust structure for Li–S batteries. The strong van der Waals stacking between the MoS<sub>2</sub> layers helps prevent the leakage/sublimation of sulfur under high vacuum environment and allows us to carefully characterize the structural change of sulfur during lithiation/delithiation with *in situ* transmission electron microscopy (TEM) ( $\sim 10^{-7}$ – $10^{-9}$  Pa). Our results provide valuable insight into the lithiation chemistry of sulfur at the nanoscale. In addition, the solution-exfoliated MoS<sub>2</sub> enables a facile synthesis method for making encapsulated sulfur particles for practical battery electrode. The novelty of this strategy lies in the following: (1) The cages formed through van der Waals stacking of the 2D MoS<sub>2</sub> flakes physically restrict the dissolution of lithium polysulfides. (2)

The as-formed wrinkles on the MoS<sub>2</sub> cages provide internal space to accommodate the volumetric change of the sulfur particles upon lithiation. (3) The favorable chemical interaction between MoS<sub>2</sub> and lithium polysulfides helps retain the active materials in the sulfur cathode. Our results show that the MoS<sub>2</sub>-encapsulated hollow sulfur sphere cathode can achieve a high specific capacity up to 1660 mAh g<sup>-1</sup> (0.1C based on sulfur mass) and long-term cycling stability with only 0.049% capacity decay per cycle over 1000 cycles at 1C.

## RESULTS AND DISCUSSION

**Hermetic Encapsulation of Sulfur Particles by Flexible MoS<sub>2</sub> Flakes.** To obtain the aqueous suspension of highly dispersed monolayer/several-layer MoS<sub>2</sub> flakes, commercial MoS<sub>2</sub> powder was first intercalated with lithium to form Li<sub>x</sub>MoS<sub>2</sub>, which was then readily exfoliated through forced hydration with the assistance of sonication.<sup>55</sup> As shown in the

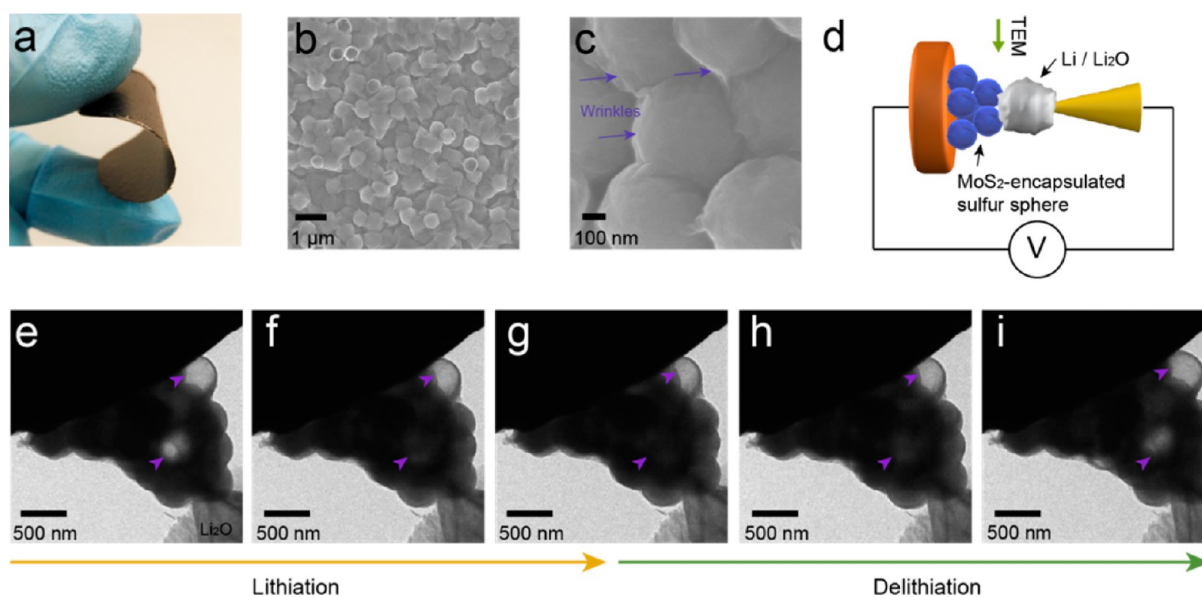


**Figure 2.** *In situ* TEM study of MoS<sub>2</sub>-encapsulated hollow sulfur spheres. (a) Photographs of a flexible film of MoS<sub>2</sub>-encapsulated hollow sulfur spheres. (b, c) SEM images of MoS<sub>2</sub>-encapsulated hollow sulfur sphere with typical wrinkles generated by the stacking of 2-D flakes marked by violet arrows in (c). (d) Schematic of *in situ* TEM setup. (e–i) Time-lapse images of the continuous lithiation and delithiation of MoS<sub>2</sub>-encapsulated hollow sulfur spheres to demonstrate the high reversibility (Movie S1).

scanning transmission electron microscopy (STEM) image (Figure 1a), the typical thickness of the MoS<sub>2</sub> flakes ranges from monolayer to several layers, with a lateral dimension of up to a few micrometers. Although some defects are observed on the flakes, the overall crystalline structure of MoS<sub>2</sub> flakes is well-preserved as shown in the high-resolution TEM images (Figure 1b). Different from its bulk properties, the 2D flakes possess good flexibility.<sup>53,56</sup> In the presence of polyvinylpyrrolidone (PVP) surfactants, MoS<sub>2</sub> flakes can self-assemble to form hollow and highly conformal cages in solution (Figures 1c and S1). Inspired by this, we developed a facile synthesis approach to prepare MoS<sub>2</sub>-encapsulated hollow sulfur spheres using the highly dispersed suspension of MoS<sub>2</sub> flakes and the PVP-encapsulated hollow sulfur spheres (Figure 1d). The PVP-sulfur particles were prepared according to a previously reported method.<sup>58</sup> Upon mixing with the PVP-sulfur suspension, the MoS<sub>2</sub> flakes would adhere to the surface of the hollow sulfur spheres due to interaction with the PVP. The van der Waals attraction between the MoS<sub>2</sub> layers allows the formation of a hermetic structure, which enables the sulfur sphere to be studied under the high vacuum TEM. The STEM image (Figure 1e), corresponding TEM image is shown in Figure S2) clearly reveals the spherical morphology of the MoS<sub>2</sub>-encapsulated hollow sulfur sphere. The energy dispersive X-ray (EDX) line scan of the sulfur signal also verifies the hollow nature of the sphere (selected area EDX spectra of MoS<sub>2</sub>-encapsulated sulfur spheres and hollow MoS<sub>2</sub> nanocages are shown in Figure S3). High-resolution TEM images indicate that the crystalline sulfur particles are conformably wrapped by few-layer (5–7 layers) stacked MoS<sub>2</sub> flakes (Figure 1f,g). As shown in Figure 1g, the van der Waal gap of typical MoS<sub>2</sub> nanocage is around 0.61 nm, and the crystalline nature of the sulfur sphere is evident by the presence of the (026) facet. With the MoS<sub>2</sub> encapsulation, the sulfur sphere can withstand 200 kV electron irradiation during TEM observation for more than 3 h and can be characterized multiple times without structural degradation. On the contrary, commercial sulfur particles

sublime very quickly (4 min) in vacuum during TEM observation, as shown in Figure S4. The XRD patterns (Figure S5) further confirm the crystallinity of the MoS<sub>2</sub> and sulfur spheres. On the basis of the TGA analysis (Figure S6), the sulfur mass loading in the MoS<sub>2</sub>-encapsulated hollow sulfur spheres is around 65%. It is interesting to note that the 2D MoS<sub>2</sub> allows the composite sulfur electrode to be highly flexible (Figure 2a). Figures 2b,c and S7 show the typical scanning electron microscopy (SEM) images of the MoS<sub>2</sub>-encapsulated hollow sulfur particle composite, which exhibit a spherical morphology and a rough surface with wrinkles (SEM images of bare sulfur sphere are shown in Figure S8). The wrinkles are likely generated from the restacking of flexible 2D flakes on the surface of sulfur spheres.

**Structural Integrity and Lithiation Dynamics of the Electrode.** The theoretical volumetric expansion of sulfur after fully being converted into Li<sub>2</sub>S is expected to be around 80%. Under normal circumstances, the large structural expansion of sulfur core will cause cracking of the outer shell. In the present design, the high flexibility of the 2D MoS<sub>2</sub> flakes allows void space to be created between the encapsulating shell and the sulfur core (Figure S9). The wrinkled MoS<sub>2</sub> coating, together with the hollow space in the sulfur core, allows effective accommodation of the volumetric expansion of sulfur spheres. To evaluate the volume expansion of MoS<sub>2</sub>-encapsulated hollow sulfur spheres, we carried out *in situ* TEM study of the sulfur lithiation process. The *in situ* TEM setup is similar to those in the previous works (Figure 2d).<sup>51,52,59–62</sup> The morphology change of the sulfur sphere is highly reversible during the lithiation and delithiation processes (Figure 2e–i, Movie S1). The hollow space inside the sulfur sphere (indicated with arrows) observed at the beginning of the reaction is gradually filled as lithiation proceeds (Figure 2e–g) to form polycrystalline Li<sub>2</sub>S as confirmed by selected area electron diffraction (SAED) and electron energy loss spectroscopy (EELS, Figure S10). When the voltage bias is reversed and the electrode is delithiated, the hollow space reappears again

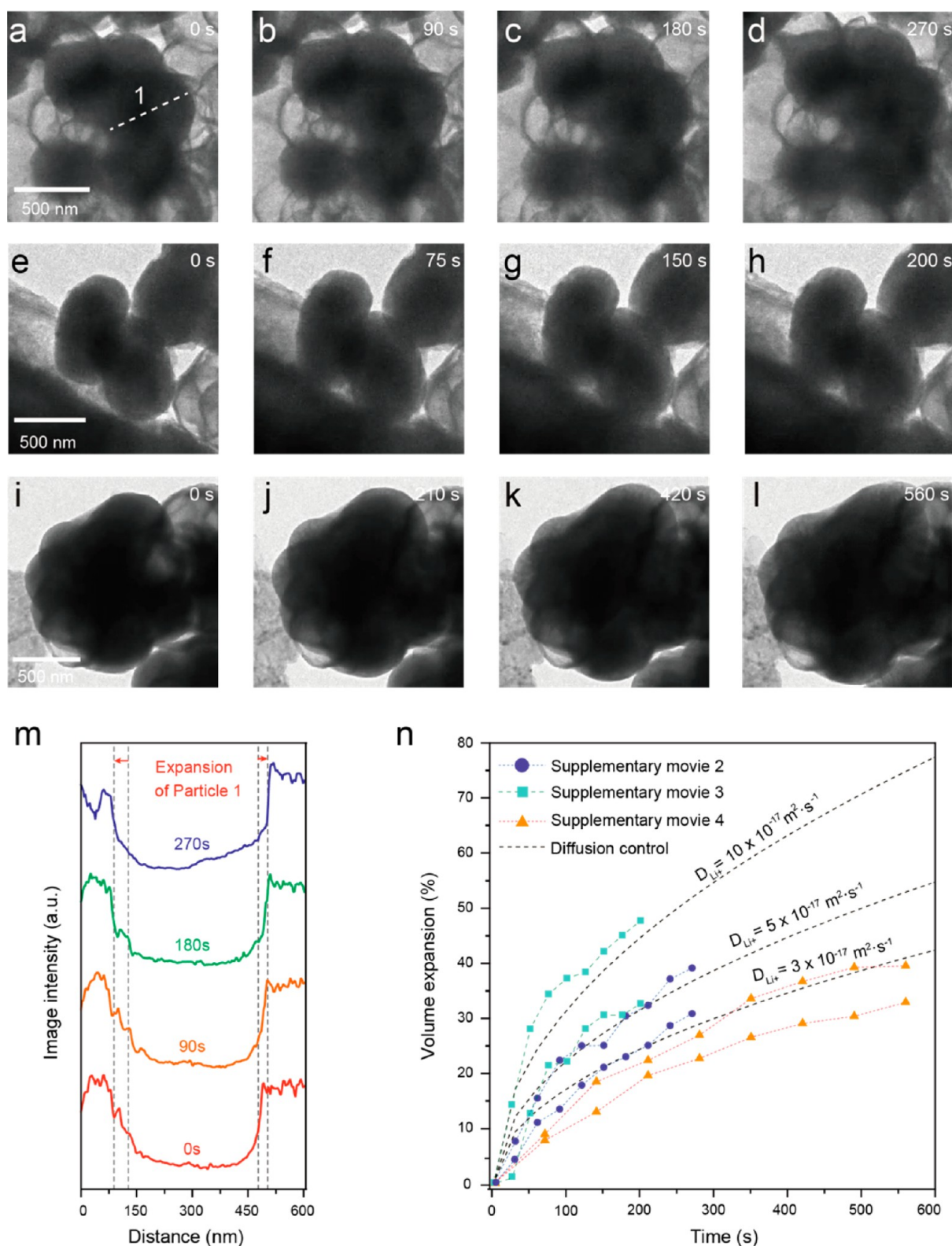


**Figure 3.** Lithium diffusion coefficient in MoS<sub>2</sub>-encapsulated hollow sulfur spheres based on *in situ* TEM study. (a–l) Time-lapse images of the lithiation of MoS<sub>2</sub>-encapsulated hollow sulfur spheres for lithium diffusion coefficient analysis (a–d: *Movie S2*, e–h: *Movie S3*, and i–l: *Movie S4*). (m) Image intensity evolution of particle 1 upon lithiation from (a–d). The volume expansion has been indicated by red arrows. (n) Lithium diffusion coefficient based on the time-dependent volume expansion measured from different particles. The measured results under *in situ* TEM indicate that the lithium diffusion coefficient in MoS<sub>2</sub>-encapsulated hollow sulfur spheres is the order of 10<sup>-17</sup>–10<sup>-16</sup> m<sup>2</sup> s<sup>-1</sup>.

(*Figure 2g–i*). This shows that in the absence of organic electrolyte, reversible lithiation and delithiation of sulfur is possible with the conductive MoS<sub>2</sub> coating. The *in situ* TEM

results are also corroborated with the *ex situ* SEM study. Typical SEM images of the sulfur composite on glassy carbon substrate before and after first lithiation (*Figure S11*) show that

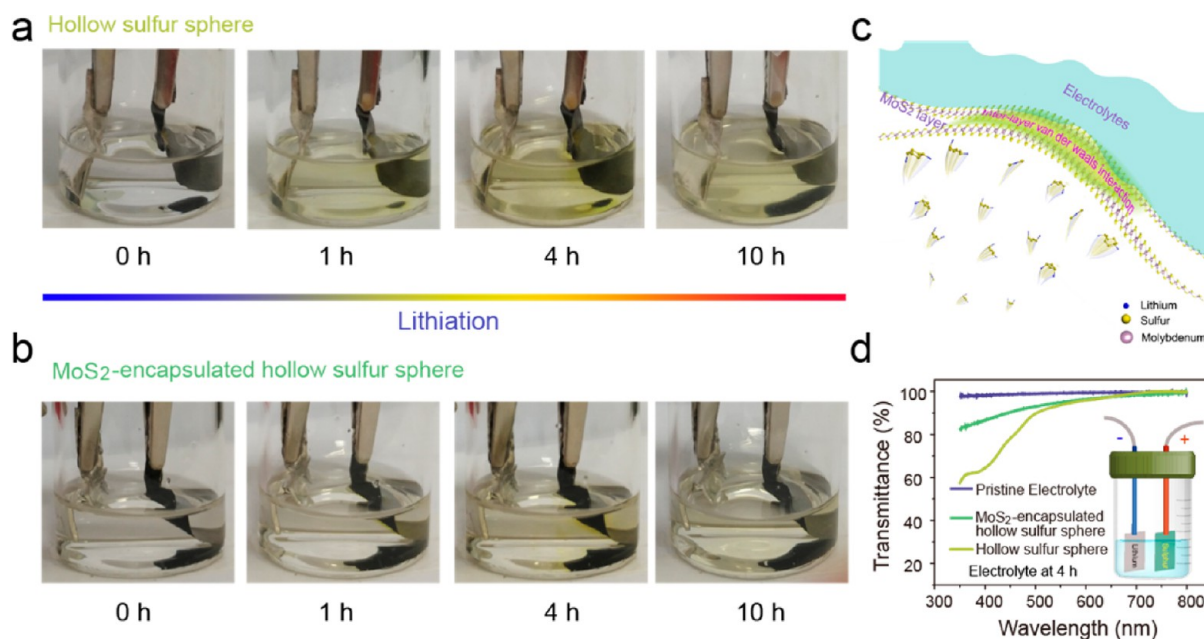


**Figure 4.** Efficient entrapment of lithium polysulfides. (a, b) Visual examination of polysulfides entrapment of (a) hollow sulfur sphere and (b)  $\text{MoS}_2$ -encapsulated hollow sulfur sphere at specific lithiation depths. (c) Schematic of the entrapment of lithium polysulfides by van der Waals stacked  $\text{MoS}_2$  cages. (d) UV-vis spectra of the electrolytes collected after 4 h of lithiation using the visual cells containing hollow sulfur sphere and  $\text{MoS}_2$ -encapsulated hollow sulfur sphere electrodes. Inset of (d) shows the schematic of visual cell configuration. These cells were discharged at 0.05C.

the structural integrity of the particles is maintained after reaction. The well-preserved particle morphology suggests that a stable electrode–electrolyte interface is maintained during the lithiation, thus limiting the leakage of lithium polysulfides into the electrolyte.

From the *in situ* TEM data, we have also analyzed the lithiation behavior of sulfur in more details (Figure 3). By plotting the line-scans of color intensity (Figure 3a,m) across the TEM images, we can measure the volume expansion of sulfur particles in different orientations. Figure 3a–l (Movies S2, S3, and S4) shows that with the hermetic encapsulation of  $\text{MoS}_2$  cages, lithiation of the sulfur sphere leads to gradual expansion of the electrode. The increase in particle size is found to be around 33 to 48%, which is smaller than the theoretical value of 80%. This could be attributed to the hollow structure of sulfur spheres that can accommodate part of the volume change and the presence of the  $\text{MoS}_2$  encapsulation layer which limits the expansion. On the basis of Fick's second law,<sup>63</sup> we estimate that the total lithium diffusivity in the encapsulated sulfur is around  $10^{-17}$ – $10^{-16}$   $\text{m}^2 \text{s}^{-1}$  (Figure 3n, detailed analysis method on the estimation of lithium diffusivity in the  $\text{MoS}_2$ -encapsulated sulfur is described in the Experimental Section), which is consistent with the previous reported values for the lithiation of spatially confined sulfur in CNTs, in which a similar type of solid-state reaction was reported.<sup>64</sup> The results show that with proper nanoscale sizing and conductive coating the rate capabilities of sulfur cathode could be comparable to that of the olivine electrode.

**Efficient Entrapment of Lithium Polysulfides.** Efficient physical confinement of sulfur and its structural integrity can provide strong entrapment of lithium polysulfides upon sulfur lithiation. To verify this, we examine the polysulfide dissolution behavior of a control sample of hollow sulfur spheres electrode and a  $\text{MoS}_2$ -encapsulated sulfur electrode using optically transparent glass cells (inset in Figure 4d). As shown in Figure

4a, the electrolyte of the cell with hollow sulfur spheres changes from colorless to the characteristic yellow polysulfide color upon partial discharge for 4 h. This corresponds to the inflection point of the discharge curve, wherein the concentration of lithium polysulfide is expected to reach the peak value.<sup>48</sup> The color change indicates that a partial dissolution of lithium polysulfide into electrolyte can still be observed in hollow sulfur spheres despite its improved electrochemical performance as compared to the commercial sulfur powder (the visual–electrochemical study of commercial sulfur powder cathode is presented in Figure S12). On the contrary, the cell with  $\text{MoS}_2$ -encapsulated hollow sulfur spheres cathode exhibits little color change at the point of discharge for 4 h, suggesting limited dissolution of lithium polysulfides in the electrolyte (Figure 4b). The UV-vis spectra (Figure 4d) of the electrolytes collected at 4 h provide further proof of a smaller amount of lithium polysulfides in the electrolyte of the cell with  $\text{MoS}_2$ -encapsulated hollow sulfur particles than that of the control sample. Upon further discharge for 10 h, while the electrolyte of the control cell remains yellow, the electrolyte of the  $\text{MoS}_2$ -encapsulated hollow sulfur electrode is colorless, indicating efficient conversion of soluble lithium polysulfides to insoluble species (i.e.,  $\text{Li}_2\text{S}_2$ ,  $\text{Li}_2\text{S}$ ). As illustrated in Figure 4c, the strong interlayer van der Waals interaction between the  $\text{MoS}_2$  flexible flakes aid in the formation of hermetic coating on the hollow sulfur spheres and effectively trap the soluble lithium polysulfide species, which agrees with the theoretical prediction based on the size of solvated soluble species as shown in Figure S13–S15 and Supporting Information section 4, theoretical understanding of the entrapment of lithium polysulfides in electrolytes and sulfur in TEM by  $\text{MoS}_2$  cages. Moreover, as compared to carbon fiber and reduced graphene oxide,  $\text{MoS}_2$  has much stronger binding with lithium polysulfides (Supporting Information section 5; discussion about the interaction between  $\text{MoS}_2$  and lithium polysulfides/sulfur, Figures S16–

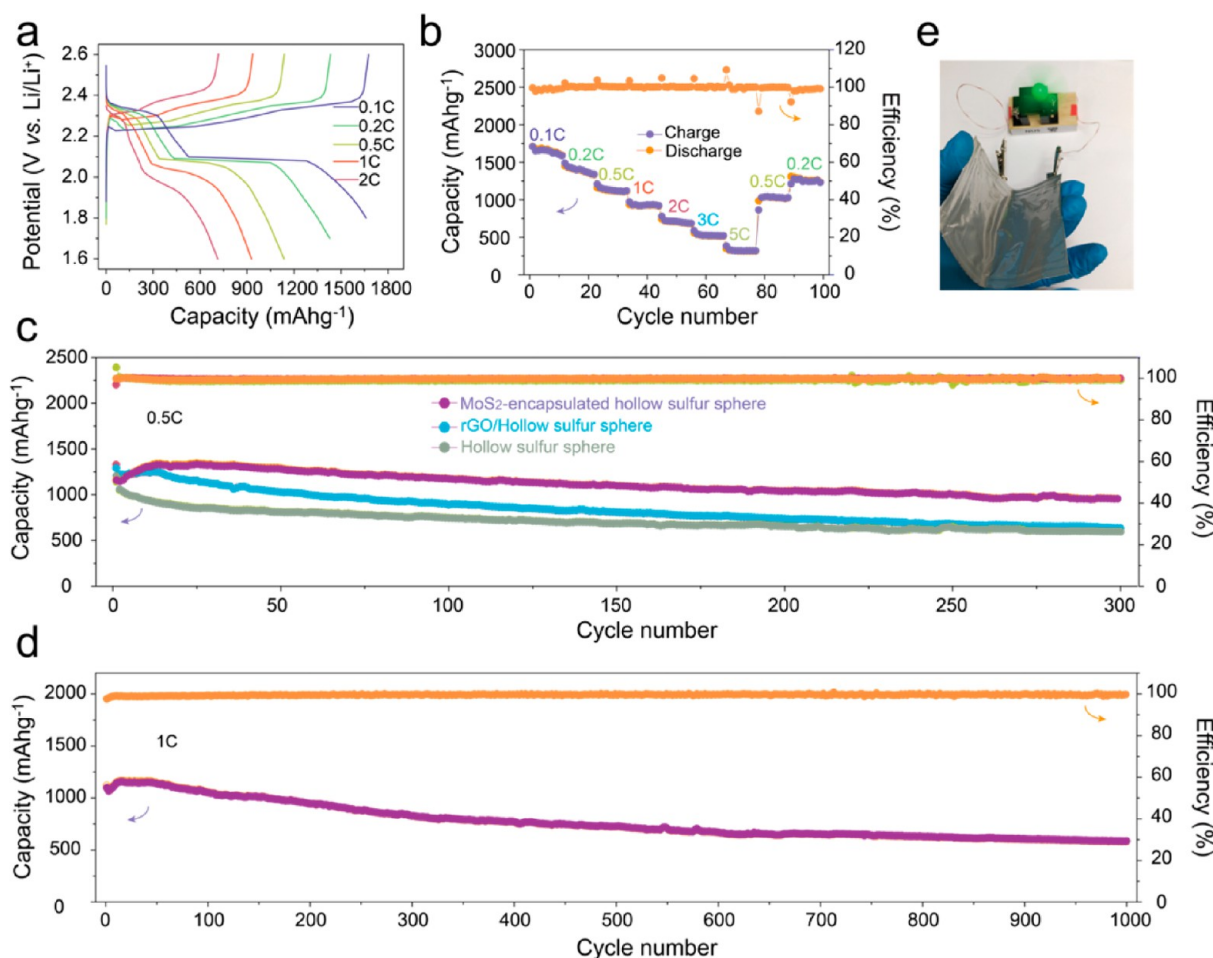


**Figure 5.** Electrochemical characterizations of MoS<sub>2</sub>-encapsulated hollow sulfur sphere. (a) Charge/discharge plots and (b) cycle capability of MoS<sub>2</sub>-encapsulated hollow sulfur sphere at different rates. (c) Long-term cycle capability of MoS<sub>2</sub>-encapsulated hollow sulfur sphere, rGO mixed with sulfur spheres and hollow sulfur sphere at 0.5C. (d) Ultra-long-term cyclability of MoS<sub>2</sub>-encapsulated hollow sulfur sphere at 1C. (e) Digital photographs of a fan powered by a pouch cell based on MoS<sub>2</sub>-encapsulated hollow sulfur sphere battery.

S21). This favorable chemical interaction provides additional entrapment of the active lithium polysulfides within the hermetic cages.

**Electrochemical Performance.** The electrochemical performance of the MoS<sub>2</sub>-encapsulated hollow sulfur sphere composite was evaluated using Li half-cells (2032-type). Working electrodes with a mass loading of  $\sim 1.5 \text{ mg cm}^{-2}$  were prepared by mixing vapor grown carbon fiber (VGCF) and polyvinylidene fluoride (PVDF) binder with the MoS<sub>2</sub>-encapsulated hollow sulfur sphere composite in *N*-methyl-2-pyrrolidone (NMP) to form a slurry. The slurry was then coated onto aluminum foil and dried under vacuum overnight. The cells were tested within a potential range of 1.8 to 2.6 V vs Li/Li<sup>+</sup> at room temperature and the specific capacity were calculated on the basis of the mass of sulfur only.

MoS<sub>2</sub>-encapsulated hollow sulfur sphere exhibits the characteristic Li–S voltage profiles when evaluated at different rate (0.1, 0.2, 0.5, 1 and 2C, wherein 1C = 1672 mAh g<sup>-1</sup>) as shown in Figure 5a. At 0.1C, the MoS<sub>2</sub>-encapsulated hollow sulfur sphere exhibits a discharge capacity of 1660 mAh g<sup>-1</sup> (based on the mass of sulfur; capacity contribution from MoS<sub>2</sub> is negligible within the operation potential window as shown in Figure S22). At higher rates of 0.2C, 0.5C, 1C, and 2C, discharge capacities of 1430, 1137, 930, and 720 mAh g<sup>-1</sup> can be obtained, respectively. When charged/discharged at higher

rates of 3C and 5C, the MoS<sub>2</sub>-encapsulated hollow sulfur sphere realizes a discharge capacity of 508 and 305 mAh g<sup>-1</sup>, respectively (Figure 5b, rate capabilities of commercial sulfur and hollow sulfur sphere are shown in Figure S23). Considering the insulating nature of sulfur and its lithiated products, such high rate capabilities of the MoS<sub>2</sub>-encapsulated sulfur electrodes are remarkable. It is noted that the semiconducting 2H-MoS<sub>2</sub> is partially transformed into the metallic 1T' phase upon lithiation (partial transformation of MoS<sub>2</sub> from 2H phase to 1T' phase upon lithiation is shown in Figures S24–S26 and Table S1) and will have a high electrical conductivity of 10–100 S cm<sup>-1</sup>.<sup>56,65–67</sup> Such high electrical conductivity may facilitate the electrochemical reaction of the insulating sulfur and its lithiated intermediate. Figure 5c shows the cycling performance of MoS<sub>2</sub>-encapsulated hollow sulfur sphere, and the control samples (hollow sulfur spheres and hollow sulfur spheres mixed with rGO) for 300 cycles at 0.5C. The discharge capacity of the MoS<sub>2</sub>-encapsulated hollow sulfur sphere electrode exhibits a gradual increase in initial cycles, which can be explained by the increase in the accessibility of sulfur to lithium ions and the gradual transformation of 2-H MoS<sub>2</sub> into 1T' metallic MoS<sub>2</sub>. Following the initial activation process, the cells made from MoS<sub>2</sub>-encapsulated hollow sulfur sphere can achieve an impressive discharge capacity up to 956 mAh g<sup>-1</sup> even after 300 cycles, showing capacity retention of

83.2% (0.056% capacity decay per cycle). SEM characterizations of MoS<sub>2</sub> encapsulated sulfur sphere electrode after extensive cycles are shown in Figure S27. Without the MoS<sub>2</sub> encapsulation, the battery cells made from hollow sulfur spheres show a quick capacity fading at the initial cycles and only 49.1% capacity retention after 300 cycles. As shown in Figure 5c, using rGO composites can partially mitigate the initial capacity fading of hollow sulfur sphere. However, the capacity retention of the cells made from rGO/hollow sulfur sphere is around 50.2% after 300 cycles with a capacity decay of 0.166% per cycle, which is similar to the hollow sulfur sphere electrodes. This indicates that rGO can only partially retain polysulfide in limited cycles.<sup>48</sup> The MoS<sub>2</sub>-encapsulated sulfur electrode shows consistently stable cycle life at high rates. The cells achieve discharge capacities up to 585 mAh g<sup>-1</sup> at 1C, with small capacity decay of 0.0449% per cycle (Figure 5d, comparison of electrochemical performance with previous sulfur-based composites shown in Table S2). The method of making the MoS<sub>2</sub> encapsulated hollow sulfur spheres can be easily scaled up (Figure S28), which will allow the practical implementation of lithium sulfur batteries (Figure 5e).

Although different processes are involved in the *in situ* TEM set up and real battery cells, both processes are controlled or partially controlled by the solid-diffusing process of lithium ion in sulfur. The fundamental problems are common to both configurations, such as the solid-state diffusion of lithium ions in sulfur composites and mitigation of local configuration changes during lithiation/delithiation. In this regard, our study about the lithium diffusion coefficient is relevant to the electrochemical behavior of sulfur-based composites and provides useful suggestions to design suitable composite electrodes for sulfur batteries.

## SUMMARY AND CONCLUSION

We have shown that by leveraging on the unique flexibility and strong interlayer van der Waals interaction of solution-exfoliated MoS<sub>2</sub> flakes, it is possible to encapsulate sulfur particles and study detailed lithiation/delithiation dynamics using *in situ* TEM. We observe that the diffusivities of lithium ion in the encapsulated sulfur particles are around 10<sup>-17</sup>–10<sup>-16</sup> m<sup>2</sup> s<sup>-1</sup>. The hermetic encapsulation of sulfur particles by MoS<sub>2</sub> cages is effective in preventing soluble lithium polysulfides from dissolution in the electrolyte, resulting in a highly reversible specific capacity up to 1660 mAh g<sup>-1</sup> at 0.1C. Moreover, owing to the internal void spaces between MoS<sub>2</sub> wrinkles and sulfur cores as well as the hollow space within the sulfur spheres, the structural integrity of the electrode can be maintained despite significant volumetric change during cycling, resulting in a stable electrode–electrolyte interface and an improved long-term cycling performance. The current study demonstrates that the unique properties of 2D materials can be exploited to address some of the material encapsulation challenges in next generation battery technologies.

## EXPERIMENTAL SECTION

**Preparation of MoS<sub>2</sub>-Encapsulated Hollow Sulfur Sphere.** Monodispersed PVP-decorated hollow sulfur spheres were prepared according to a previous report.<sup>56</sup> In a typical synthesis, 100 mL of 0.08 M sodium thiosulfate (8 mmol, 99%, Sigma-Aldrich) solution was drop-wised mixed with 100 mL 0.4 M PVP (40 mmol, Sigma-Aldrich,  $M_w \approx 55\,000$ , the concentration was calculated in terms of the repeating unit) solution. After stirring for 15 min, 0.8 mL of concentrated hydrochloric acid (HCl, 36.5–38.0%, Sigma-Aldrich)

was added to the mixture. After stirring for 2 h at room temperature, the product was collected by centrifugation at 7000 rpm for 10 min. The product was then redispersed in 0.4 M PVP solution and recollected by centrifugation at 6000 rpm for 10 min. The mass of sulfur particle collected in this process is around 100 mg. The product was dispersed again in distilled water for use (solution A, with a concentration around 4 mg mL<sup>-1</sup>). MoS<sub>2</sub> dispersion was prepared through forced hydration of lithium intercalated MoS<sub>2</sub> with the assistant of sonication. Lithium intercalation was achieved by stirring 2 g of natural MoS<sub>2</sub> crystals (99%, Sigma-Aldrich) in 20 mL of 1.6 M butyllithium solution in anhydrous hexane (32 mmol, Sigma-Aldrich) for 3 days in an argon-filled glovebox. Li<sub>x</sub>MoS<sub>2</sub> was retrieved by filtration and washed with anhydrous hexane to remove excess lithium and organic residues. After being dried in vacuum, exfoliation was achieved immediately after this by ultrasonating Li<sub>x</sub>MoS<sub>2</sub> in water for 1 h. After dialyzing for 4 days, the suspension of MoS<sub>2</sub> flakes was collected for use with a concentration around 1 mg mL<sup>-1</sup> (solution B). Solution A (20 mL) was then added drop by drop to 40 mL of solution B under stirring. After stirring for 1 h, the black suspension was filtrated and washed by water/methanol 3 times to collect the MoS<sub>2</sub>-encapsulated hollow sulfur sphere product. Hollow sulfur sphere product was collected by vacuum filtration of solution A and washed by water/methanol. The isolated yield of MoS<sub>2</sub>-encapsulated hollow sulfur sphere product from this small batch is around 130–140 mg. With the help of our industrial partner, the batch can be scaled up, and the yield can be improved to 10 g.

### Estimation of Lithium Diffusivity in the Encapsulated Sulfur.

To estimate the lithium diffusivity in the MoS<sub>2</sub>-encapsulated sulfur spheres, the TEM image line scans governed by various lithium diffusivities through finite-difference simulations from Fick's second law were simulated. For the finite-difference simulations, a sphere was broken into radial shell units and numerically solved for the concentration in each unit over a series of time steps. The model has been detailed in our previous work as discussed in the Supporting Information.<sup>57</sup> From these concentration profiles, according TEM image intensity line scans were calculated based on mass–thickness contrast governed by different lithium diffusivities. By comparing the experimental TEM image line scans with the simulated results, we can estimate the lithium diffusivity in MoS<sub>2</sub>-encapsulated sulfur spheres.

***In Situ* TEM.** A specialized dual-probe electrical biasing holder (Nanofactory Instruments) was used. The voltage bias was set as 2 or –1.5 V versus the counter electrode for lithiation/delithiation. Li<sup>+</sup> flow through the oxide/nitride layer and are reduced at the working electrode, where they react MoS<sub>2</sub>-encapsulated hollow sulfur sphere.

## ASSOCIATED CONTENT

### Supporting Information

The Supporting Information is available free of charge on the ACS Publications website at DOI: 10.1021/jacs.7b05371.

Detailed experimental descriptions, phase evolution of MoS<sub>2</sub>-encapsulated hollow sulfur, theoretical understanding and discussion about interaction between MoS<sub>2</sub> and lithium polysulfides in the electrolyte and TEM, and characterization of MoS<sub>2</sub>-encapsulated sulfur sphere electrodes after extensive cycles (PDF)

Movie S1: continuous lithiation and delithiation of MoS<sub>2</sub>-encapsulated hollow sulfur spheres to demonstrate the high reversibility (MPG)

Movies S2–S4: lithiation of MoS<sub>2</sub>-encapsulated hollow sulfur spheres for lithium diffusion coefficient analysis (MPG, MPG, and MPG)

## AUTHOR INFORMATION

### Corresponding Authors

\*hyunwooklee@unist.ac.kr

\*chmlhkp@nus.edu.sg

\*wesley-zheng@imre.a-star.edu.sg

**ORCID**

Wei Tang: 0000-0001-7154-4089

Xiaofeng Fan: 0000-0001-6288-4866

Meng Li: 0000-0003-0087-3082

Jianyi Chen: 0000-0002-3757-7634

Kian Ping Loh: 0000-0002-1491-743X

**Author Contributions**

W.T., Z.C., and B.T. contributed equally to this work.

**Notes**

The authors declare no competing financial interest.

**ACKNOWLEDGMENTS**

We acknowledge support by NRF-CRP “Novel 2-D Materials with Tailored Properties: Beyond Graphene R-143-000-295-281”. The electron microscopy work was supported in part by the U.S. Department of Energy (DOE), Office of Science, Basic Energy Science, Materials Sciences and Engineering Division (W.Z.) and through a user project at ORNL’s Center for Nanophase Materials Sciences (CNMS), which is a DOE Office of Science User Facility. G.Z., W.T., and X.Y. acknowledge support from Guangdong Dynavolt Renewable Energy Technology Co Ltd. H.-W.L. acknowledges support from Basic Science Research Program through the National Research Foundation of Korea funded by the Ministry of Education (2016R1C1B2013935). Q.Z. thanks for support the Specialized Research Fund for the Doctoral Program of Higher Education of China (Grant No. NRF-20131102120001) and the program for New Century Excellent Talents in University (Grant No. NCET-12-0033).

**REFERENCES**

- (1) Armand, M.; Tarascon, J. M. *Nature* **2008**, *451*, 652–657.
- (2) Goodenough, J. B. *Energy Environ. Sci.* **2014**, *7*, 14–18.
- (3) Thackeray, M. M.; Wolverton, C.; Isaacs, E. D. *Energy Environ. Sci.* **2012**, *5*, 7854–7863.
- (4) Lin, M.-C.; Gong, M.; Lu, B.; Wu, Y.; Wang, D.-Y.; Guan, M.; Angell, M.; Chen, C.; Yang, J.; Hwang, B.-J.; Dai, H. *Nature* **2015**, *520*, 324–328.
- (5) Bachman, J. C.; Kaviani, R.; Graham, D. J.; Kim, D. Y.; Noda, S.; Nocera, D. G.; Shao-Horn, Y.; Lee, S. W. *Nat. Commun.* **2015**, *6*, 7040.
- (6) Suo, L.; Hu, Y.-S.; Li, H.; Armand, M.; Chen, L. *Nat. Commun.* **2013**, *4*, 1481.
- (7) Lim, H.-D.; Lee, B.; Zheng, Y.; Hong, J.; Kim, J.; Gwon, H.; Ko, Y.; Lee, M.; Cho, K.; Kang, K. *Nat. Energy* **2016**, *1*, 16066.
- (8) Wu, Z.-S.; Tan, Y.-Z.; Zheng, S.; Wang, S.; Parvez, K.; Qin, J.; Shi, X.; Sun, C.; Bao, X.; Feng, X.; Müllen, K. *J. Am. Chem. Soc.* **2017**, *139*, 4506–4512.
- (9) Yang, P.; Tarascon, J.-M. *Nat. Mater.* **2012**, *11*, 560–563.
- (10) Huang, C.; Xiao, J.; Shao, Y.; Zheng, J.; Bennett, W. D.; Lu, D.; Saraf, L. V.; Engelhard, M.; Ji, L.; Zhang, J.; Li, X.; Graff, G. L.; Liu, J. *Nat. Commun.* **2014**, *5*, 3015.
- (11) Borchardt, L.; Oschatz, M.; Kaskel, S. *Chem. - Eur. J.* **2016**, *22*, 7324–7351.
- (12) Evers, S.; Nazar, L. F. *Acc. Chem. Res.* **2013**, *46*, 1135–1143.
- (13) Pang, Q.; Liang, X.; Kwok, C. Y.; Nazar, L. F. *Nat. Energy* **2016**, *1*, 16132.
- (14) Rehman, S.; Guo, S.; Hou, Y. *Adv. Mater.* **2016**, *28*, 3167–3172.
- (15) Peng, H.-J.; Huang, J.-Q.; Liu, X.-Y.; Cheng, X.-B.; Xu, W.-T.; Zhao, C.-Z.; Wei, F.; Zhang, Q. *J. Am. Chem. Soc.* **2017**, *139*, 8458–8466.
- (16) Xu, Y.; Wen, Y.; Zhu, Y.; Gaskell, K.; Cychosz, K. A.; Eichhorn, B.; Xu, K.; Wang, C. *Adv. Funct. Mater.* **2015**, *25*, 4312–4320.

- (17) Jayaprakash, N.; Shen, J.; Moganty, S. S.; Corona, A.; Archer, L. A. *Angew. Chem., Int. Ed.* **2011**, *50*, 5904–5908.
- (18) Liang, C.; Dudney, N. J.; Howe, J. Y. *Chem. Mater.* **2009**, *21*, 4724–4730.
- (19) Ji, X.; Lee, K. T.; Nazar, L. F. *Nat. Mater.* **2009**, *8*, 500–506.
- (20) Li, Z.; Zhang, J.; Guan, B.; Wang, D.; Liu, L.-M.; Lou, X. W. *Nat. Commun.* **2016**, *7*, 13065.
- (21) Wang, H.; Zhang, W.; Liu, H.; Guo, Z. *Angew. Chem., Int. Ed.* **2016**, *55*, 3992–3996.
- (22) Zhang, J.; Yang, C.-P.; Yin, Y.-X.; Wan, L.-J.; Guo, Y.-G. *Adv. Mater.* **2016**, *28*, 9539–9544.
- (23) Guo, J.; Xu, Y.; Wang, C. *Nano Lett.* **2011**, *11*, 4288–4294.
- (24) Elazari, R.; Salitra, G.; Garsuch, A.; Panchenko, A.; Aurbach, D. *Adv. Mater.* **2011**, *23*, 5641–5644.
- (25) Zhou, G.; Wang, D.-W.; Li, F.; Hou, P.-X.; Yin, L.; Liu, C.; Lu, G. Q.; Gentle, I. R.; Cheng, H.-M. *Energy Environ. Sci.* **2012**, *5*, 8901–8906.
- (26) Xin, S.; Gu, L.; Zhao, N.-H.; Yin, Y.-X.; Zhou, L.-J.; Guo, Y.-G.; Wan, L.-J. *J. Am. Chem. Soc.* **2012**, *134*, 18510–18513.
- (27) Li, W.; Zhang, Q.; Zheng, G.; Seh, Z. W.; Yao, H.; Cui, Y. *Nano Lett.* **2013**, *13*, 5534–5540.
- (28) Zhou, W.; Yu, Y.; Chen, H.; DiSalvo, F. J.; Abruña, H. D. *J. Am. Chem. Soc.* **2013**, *135*, 16736–16743.
- (29) Fu, Y.; Manthiram, A. *J. Phys. Chem. C* **2012**, *116*, 8910–8915.
- (30) Zhou, W.; Xiao, X.; Cai, M.; Yang, L. *Nano Lett.* **2014**, *14*, 5250–5256.
- (31) Zhang, Y.; Zhao, Y.; Yermukhambetova, A.; Bakenov, Z.; Chen, P. *J. Mater. Chem. A* **2013**, *1*, 295–301.
- (32) Kim, H.; Lee, J.; Ahn, H.; Kim, O.; Park, M. J. *Nat. Commun.* **2015**, *6*, 7278.
- (33) Wei, S.; Ma, L.; Hendrickson, K. E.; Tu, Z.; Archer, L. A. *J. Am. Chem. Soc.* **2015**, *137*, 12143–12152.
- (34) Wang, H.; Yang, Y.; Liang, Y.; Robinson, J. T.; Li, Y.; Jackson, A.; Cui, Y.; Dai, H. *Nano Lett.* **2011**, *11*, 2644–2647.
- (35) Ji, L.; Rao, M.; Zheng, H.; Zhang, L.; Li, Y.; Duan, W.; Guo, J.; Cairns, E. J.; Zhang, Y. *J. Am. Chem. Soc.* **2011**, *133*, 18522–18525.
- (36) Ding, Y.-L.; Kopold, P.; Hahn, K.; van Aken, P. A.; Maier, J.; Yu, Y. *Adv. Funct. Mater.* **2016**, *26*, 1112–1119.
- (37) Wang, Z.; Dong, Y.; Li, H.; Zhao, Z.; Bin Wu, H.; Hao, C.; Liu, S.; Qiu, J.; Lou, X. W. *Nat. Commun.* **2014**, *5*, 5002.
- (38) Zhao, M.-Q.; Zhang, Q.; Huang, J.-Q.; Tian, G.-L.; Nie, J.-Q.; Peng, H.-J.; Wei, F. *Nat. Commun.* **2014**, *5*, 3410.
- (39) Chen, H.; Wang, C.; Dai, Y.; Qiu, S.; Yang, J.; Lu, W.; Chen, L. *Nano Lett.* **2015**, *15*, 5443–5448.
- (40) Al Salem, H.; Babu, G.; Rao, C. V.; Arava, L. M. R. *J. Am. Chem. Soc.* **2015**, *137*, 11542–11545.
- (41) Wang, X.; Li, G.; Li, J.; Zhang, Y.; Wook, A.; Yu, A.; Chen, Z. *Energy Environ. Sci.* **2016**, *9*, 2533–2538.
- (42) Jiang, J.; Zhu, J.; Ai, W.; Wang, X.; Wang, Y.; Zou, C.; Huang, W.; Yu, T. *Nat. Commun.* **2015**, *6*, 8622.
- (43) Zhang, S. S.; Tran, D. T. *J. Mater. Chem. A* **2016**, *4*, 4371–4374.
- (44) Yuan, Z.; Peng, H.-J.; Hou, T.-Z.; Huang, J.-Q.; Chen, C.-M.; Wang, D.-W.; Cheng, X.-B.; Wei, F.; Zhang, Q. *Nano Lett.* **2016**, *16*, 519–527.
- (45) Li, Y.-J.; Fan, J.-M.; Zheng, M.-S.; Dong, Q.-F. *Energy Environ. Sci.* **2016**, *9*, 1998–2004.
- (46) Bai, S.; Liu, X.; Zhu, K.; Wu, S.; Zhou, H. *Nat. Energy* **2016**, *1*, 16094.
- (47) Lee, J. T.; Zhao, Y.; Thieme, S.; Kim, H.; Oschatz, M.; Borchardt, L.; Magasinski, A.; Cho, W.-I.; Kaskel, S.; Yushin, G. *Adv. Mater.* **2013**, *25*, 4573–4579.
- (48) Liang, X.; Hart, C.; Pang, Q.; Garsuch, A.; Weiss, T.; Nazar, L. F. *Nat. Commun.* **2015**, *6*, 5682.
- (49) Zheng, J.; Tian, J.; Wu, D.; Gu, M.; Xu, W.; Wang, C.; Gao, F.; Engelhard, M. H.; Zhang, J.-G.; Liu, J.; Xiao, J. *Nano Lett.* **2014**, *14*, 2345–2352.
- (50) Mao, Y.; Li, G.; Guo, Y.; Li, Z.; Liang, C.; Peng, X.; Lin, Z. *Nat. Commun.* **2017**, *8*, 14628.

- (51) Kim, H.; Lee, J. T.; Magasinski, A.; Zhao, K.; Liu, Y.; Yushin, G. *Adv. Energy Mater.* **2015**, *5*, 1501306.
- (52) Yang, Z.; Zhu, Z.; Ma, J.; Xiao, D.; Kui, X.; Yao, Y.; Yu, R.; Wei, X.; Gu, L.; Hu, Y.-S.; Li, H.; Zhang, X. *Adv. Energy Mater.* **2016**, *6*, 1600806.
- (53) Yuk, J. M.; Park, J.; Ercius, P.; Kim, K.; Hellebusch, D. J.; Crommie, M. F.; Lee, J. Y.; Zettl, A.; Alivisatos, A. P. *Science* **2012**, *336*, 61–64.
- (54) Zhao, J.; Deng, Q.; Avdoshenko, S. M.; Fu, L.; Eckert, J.; Rümmeli, M. H. *Proc. Natl. Acad. Sci. U. S. A.* **2014**, *111*, 15641–15646.
- (55) Eda, G.; Yamaguchi, H.; Voiry, D.; Fujita, T.; Chen, M.; Chhowalla, M. *Nano Lett.* **2011**, *11*, 5111–5116.
- (56) Acerce, M.; Voiry, D.; Chhowalla, M. *Nat. Nanotechnol.* **2015**, *10*, 313–318.
- (57) McDowell, M. T.; Lee, S. W.; Harris, J. T.; Korgel, B. A.; Wang, C.; Nix, W. D.; Cui, Y. *Nano Lett.* **2013**, *13*, 758.
- (58) Li, W.; Zheng, G.; Yang, Y.; Seh, Z. W.; Liu, N.; Cui, Y. *Proc. Natl. Acad. Sci. U. S. A.* **2013**, *110*, 7148–7153.
- (59) Huang, J. Y.; Zhong, L.; Wang, C. M.; Sullivan, J. P.; Xu, W.; Zhang, L. Q.; Mao, S. X.; Hudak, N. S.; Liu, X. H.; Subramanian, A.; Fan, H.; Qi, L.; Kushima, A.; Li, J. *Science* **2010**, *330*, 1515–1520.
- (60) Liu, X. H.; Wang, J. W.; Huang, S.; Fan, F.; Huang, X.; Liu, Y.; Krylyuk, S.; Yoo, J.; Dayeh, S. A.; Davydov, A. V.; Mao, S. X.; Picraux, S. T.; Zhang, S.; Li, J.; Zhu, T.; Huang, J. Y. *Nat. Nanotechnol.* **2012**, *7*, 749–756.
- (61) Wang, Z.; Santhanagopalan, D.; Zhang, W.; Wang, F.; Xin, H. L.; He, K.; Li, J.; Dudney, N.; Meng, Y. S. *Nano Lett.* **2016**, *16*, 3760–3767.
- (62) Wang, F.; Yu, H.-C.; Chen, M.-H.; Wu, L.; Pereira, N.; Thornton, K.; Van der Ven, A.; Zhu, Y.; Amatucci, G. G.; Graetz, J. *Nat. Commun.* **2012**, *3*, 1201.
- (63) McDowell, M. T.; Ryu, I.; Lee, S. W.; Wang, C.; Nix, W. D.; Cui, Y. *Adv. Mater.* **2012**, *24*, 6034–6041.
- (64) Yang, C.-P.; Yin, Y.-X.; Guo, Y.-G.; Wan, L.-J. *J. Am. Chem. Soc.* **2015**, *137*, 2215–2218.
- (65) Cook, J. B.; Kim, H.-S.; Yan, Y.; Ko, J. S.; Robbennolt, S.; Dunn, B.; Tolbert, S. H. *Adv. Energy Mater.* **2016**, *6*, 1501937.
- (66) Xiong, F.; Wang, H.; Liu, X.; Sun, J.; Brongersma, M.; Pop, E.; Cui, Y. *Nano Lett.* **2015**, *15*, 6777–6784.
- (67) Zeng, Z.; Zhang, X.; Bustillo, K.; Niu, K.; Gammer, C.; Xu, J.; Zheng, H. *Nano Lett.* **2015**, *15*, 5214–5220.